Available online at www.sciencedirect.com
ScienceDirect
Physics Procedia 00 (2012) 1–8
Physics Procedia

TIPP 2011 - Technology and Instrumentation in Particle Physics 2011

An Application of Micro-channel Plate Photomultiplier Tube to Positron Emission Tomography

H. Kim[a,*], C.-T. Chen[a], H. Frisch[b], F. Tang[b], C.-M. Kao[a]

[a] *Department of Radiology, University of Chicago, Chicago, IL 60637*
[b] *Enrico Fermi Institute, University of Chicago, Chicago, IL 60637*

Abstract

We are developing a Time-of-Flight Positron Emission Tomography detector using flat panel micro-channel plate photomultiplier tubes (MCP PMT). The high-speed waveform sampling data acquisition is adopted to exploit the fast time response of MCP PMT efficiently by using transmission-line readout scheme. To demonstrate the feasibility of the proposed detector, prototype detector modules were built using Photonis XP85022 MCP PMT, transmission-line board (TL), and high-speed waveform sampling electronics equipped with DRS4 chips. The MCP/TL module was coupled to single LYSO crystal, and experimental tests have been conducted in a coincidence setup to measure the responses to 511 keV annihilation photon. The details of the prototype module, experimental setup, and the preliminary results are presented and discussed.

Keywords: Positron Emission Tomography, Micro-Channel Plate Photomultiplier, Transmission-Line Readout, Waveform Sampling, Time Resolution
PACS: 87.57.uk, 85.60.Gz, 84.40.Az, 29.40.Mc

1. Introduction

Positron Emission Tomography (PET) is a medical imaging modality to show the distribution of radio-tracer in organs, and give metabolic activity by detecting two annihilation photons from positron emitting nuclides. To conserve energy during positron annihilation, two out-coming photons move in nearly opposite direction with the energy of 511 keV. Positron annihilation events are tagged by detection of two 511 keV gamma at the same time, typically ~10 ns of time window. As the new fast scintillators and electronics for time measurement are developed, it becomes possible to localize the positron decay position within the detection time resolution: Time-of-Flight PET (TOF PET) [1] [2], and thereby result in noise reduction in the image reconstruction. The benefits of using TOF PET include image quality improvement, reduction of the image scanning time, dose reduction, and increasing throughput, etc. Current commercial clinical TOF PET scanners have reported 550~600 ps [3][4] of coincidence time resolution. To improve the coincidence time resolution while keeping or increasing detection efficiency is the key issues in TOF PET instrumentation research.

*Corresponding author
Email address: heejongkim@uchicago.edu (H. Kim)

We have proposed a design of TOF PET detector employing the new technologies. The conceived TOF PET design has three distinctive features compared to the conventional PET detectors. (1)Firstly, flat panel micro-channel plate photomultiplier tube (MCP PMT) [5] is adopted rather than commonly used PMT in our design. MCP PMT is fast [6][7], position sensitive, compact in size, and less sensitive in the magnetic field [8]. These characteristics of MCP PMT would enable various new PET detector configurations that can hardly be realized with the conventional PMTs. The 8"x8" flat panel MCP PMT, which is currently under development by the LAPPD project [9], would be suitable for the PET application. (2)The transmission-line readout scheme [10] utilizing fast timing of MCP PMT is another new feature implemented in the design. In this readout scheme, the electrical signals of MCP PMT are formed and transported on the anode strips running in parallel. Event position in one direction is obtained from the strip-line coordinates weighted with their signal amplitudes. And the time difference of correlated signal on the same strip-line makes it possible to extract the event position along the strip-line. In this way the number of electronics channels can be reduced efficiently, especially for large area signal readout. (3)High-speed waveform sampling (≥5 GS/s) is introduced to achieve precise time decision from the fast MCP PMT signal [11]. Conventional PET data acquisition uses two signal digitization chains by splitting the PMT output, one for energy measurement using ADC, and the other for time decision using TDC. This complexity can be avoided in waveform sampling readout: all the event information is obtained in an unified way by processing the digitized waveform. The digitized waveform processing provides more flexibilities in event handling, e.g., offset shift on base-line or pile-up events in high count rate condition.

The conceptual drawing of the PET detector design implementing these features is shown in Figure. 1. The detector in the drawing consists of two modules, in each module an array of scintillator is coupled by two large area flat panel MCP PMTs. In addition to the 2-dimensional event position, the depth of interaction (DOI) is obtained by using two MCP PMTs at both sides. Due to compact thickness of MCP PMT, the sensitivity of the detector can be increased easily by stacking multiple layers of the module. A simulation study [12] was conducted to investigate the feasibility of the design concept, and the results of the study show that the proposed design based on the flat panel MCP PMT is suitable for TOF PET detector. We have developed prototype PET detector modules and made experimental tests to demonstrate the idea based on the MCP PMT, transmission-line readout and waveform sampling. In the following sections, the technical details of the prototype module and experimental tests are described, and some preliminary results are presented.

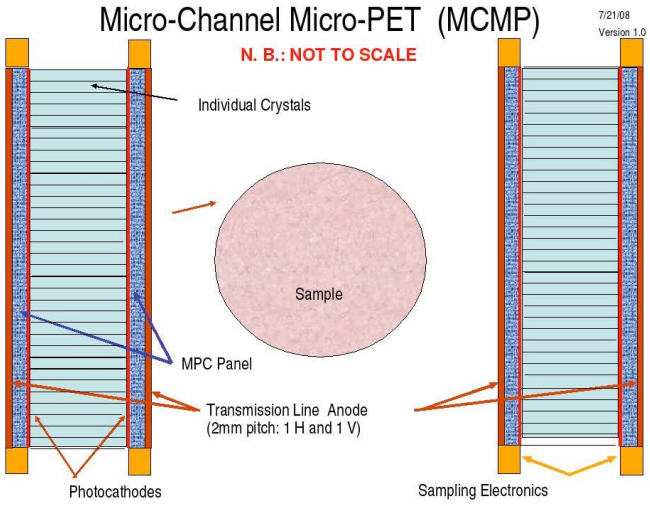

Figure 1. A conceptual drawing of the PET detector using flat panel MCP PMTs. One detector module consists of an array of pixelated scintillators and two MCP PMT panels. The high-speed sampling electronics digitize waveforms of transmission-line signal at both ends of the strips.

2. Materials and Methods

2.1. A Prototype Module

The prototype detector module is built by using XP85022 from Photonis [13] and transmission-line board. The XP85022 is a 2"x2" flat panel MCP PMT which has two layers of MCP (chevron) with 25 μm diameter of pore; the length-to-diameter ratio (L/D) is 40. The quantum efficiency of XP8022 is ~24% at 400 nm wavelength. The anode of XP85022 has 32x32 array structure with 1.1 mm size and 1.6 mm pitch. The electrical signals from the XP85022 anode are collected on the strips on the transmission-line board. The transmission board has 32 strips running in parallel with 1.6 mm pitch to match the anode structure of XP85022. The board has 32 connecting points at both ends of the strip for signal readout. The signal propagation speed on the strip-line is measured to be 0.46 c (c is a speed of light in vacuum) using a collimated light emitting diode [14]. Figure 2(a) shows the anode structure of the XP85022 and transmission line board before assembly .

The waveform from the strips of the transmission-line board are recorded by the prototype readout board using the DRS4 chip [15]. DRS4 is the high speed waveform sampling chip based on Switched Capacitor Arrays (SCA) technology, and provides nine channels each with 1024 capacitor cells. The input dynamic range of the DRS4 is 1 V, and the maximum sampling speed is ~5 giga-samples per second (GS/s). The prototype readout board has eight channels in a 7"x8.75" PCB board. Signal inputs is amplified with 5 times fixed gain (LMH6702MF) and fed to analog memory buffers of DRS4 chip for sampling. With trigger signals, writing to analog buffer memories are stopped and digitized by 12 bit octal ADC (AD9222, Analog Devices) in parallel. The digital memory buffer stores 8 events per channel; each event has size of 1024 x 12 bit. The trigger of the board is made by external or a combination of discriminators of eight input channels. ADC and memory buffer are controlled by Xilinx FPGA (XC5VLX30T-1FF665C). The prototype readout board is shown in Figure 2(b).

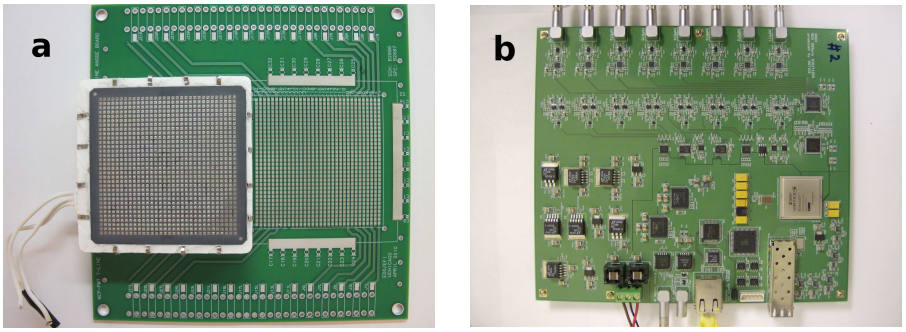

Figure 2. (a) A prototype detector module before assembly. A XP85022 MCP PMT showing anode array structure is placed on top of the transmission-line board. The 32 strip-lines of the board can be connected to DRS4 inputs through LEMO cables. (b) A waveform readout board employing the DRS4 chip provides eight input channels for waveform sampling, an external trigger, and an Ethernet interface.

2.2. Experimental Setup

The experimental setup consists of a MCP PMT/TL module and Hamamatsu R9800 PMT. A single LYSO crystal with dimension of 3x3x10 mm^3 (Proteus Inc.) is optically coupled to the window of MCP PMT/TL via a 3x3 mm^2 side, and other sides of the crystal are wrapped by white Teflon tape. A Fluke 415B power supply unit provides -2350 V of high voltage to MCP PMT/TL module; the MCP gain is estimated to $2x10^6$ at the applied voltage. For a coincidence detector, the R9800 PMT is coupled with an LSO crystal with 6.2x6.2x25 mm^3, and -1000 V of high voltage is applied by another Fluke 415B unit. The smaller gain of the PMT with the lower high voltage is compensated by the embedded amplifier in the readout board to keep the overall gain at $\sim 10^6$. Two detector modules are located 7 cm away from each other, and a ^{22}Na source with a 0.25 mm active diameter is placed in the middle of the two modules as a positron annihilation source. Figure 3(a) shows the MCP PMT/TL module and R9800 PMT in coincidence setup.

The output signals from the MCP PMT/TL module and R9800 PMT are readout by two readout board providing 16 input channels in total; one channel is assigned to the R9800 PMT, and the other 15 channels are connected to the

strips from the MCP PMT/TL module. External trigger signal for the readout board is prepared by using Lecroy 622 coincidence unit and 623B discriminators; 50 mV and 100 mV thresholds are set for the R9800 PMT and sum of four strips from MCP PMT/TL module, respectively. Waveforms from the detector modules are sampled at 5 GS/s. The block diagram to depict the experimental setup is shown in Figure 3(b).

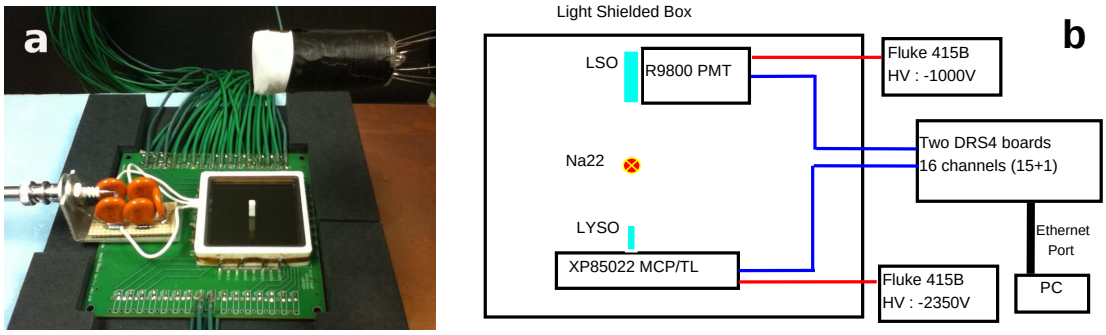

Figure 3. (a) Two detector modules in coincidence setup. A MCP PMT/TL module after assembly is placed on the bottom, and a Hamamatsu R9800 PMT is used as coincidence detector. (b) A block diagram of the experimental setup.

2.3. Waveform Processing

The waveforms sampled by the readout boards are stored in hard disk for off-line analysis. One coincidence event consists of 16 set of waveform, each waveform having 1024 sampling points with ~200 ps, thus having ~200 ns of sampling interval. Figure 4 shows an example waveform on a strip from the MCP PMT/TL. The polarity of the waveform is inverted for display purpose in the figure. The waveform processing to get the event information can be summarized as follows.

(a) Base-line correction: the sampled point in the first 20 ns in the waveform is used for offset shift of the base-line. The base-line correction is made for each waveform.

(b) Photon energy: the energy deposition of annihilation photon is estimated by the area integration of waveform. Pulse amplitudes of the sampled point are summed up for 150 ns, from the pulse starting point.

(c) Event time: the event time uses only the rising part of the waveform. A low-pass filter is applied to reduce high-frequency noise in the 20 ns length sub-waveform around the rising part. The sub-waveform is up-sampled to have ~10 ps sampling interval by using cubic-spline interpolation algorithm [16]. Two kinds of time pick-up are applied on the newly interpolated waveform for determining event time: the leading-edge discriminator (d-LED) and the constant-fraction discriminator (d-CFD) are implemented. d-LED uses a fixed threshold, while the threshold in d-CFD can vary depending on the pulse amplitude. Time crossing the threshold is calculated from the linear interpolation between two adjacent points around the threshold amplitude. Figure 4(b) shows the close-up of rising part of the waveform in Figure 4(a), and describes how d-LED and d-CFD determine the event time.

(d) Position: the crystal position along the strip direction is calculated from the time difference measured at two ends of the transmission-line strip. The two waveforms propagating toward the ends are identical in shape and amplitude. A new time pick-up method is developed to exploit the correlation of two waveforms; multiple leading-edge discriminator (m-LED) uses several different thresholds on the rising part of waveform. The averaged time difference measured at multiple thresholds is more accurate than the ones using single threshold. The crystal position perpendicular to the strip direction is obtained from the strips' coordinates weighted by the signal amplitude.

3. Results

3.1. Performances of the waveform sampling readout board

Amplitude calibration of the readout board is carried out for all the capacitor cells by varying offset voltages in range [-0.45V, 0.45V]: the offset voltage range [-0.5V, 0.5V] can be controlled by the 12 bit DAC value. The offsets

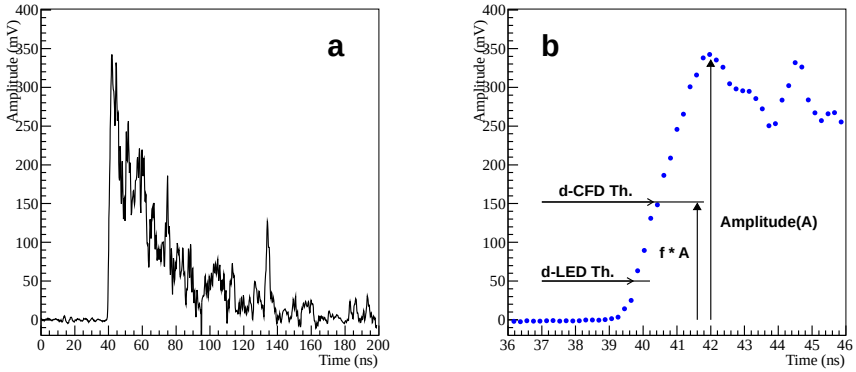

Figure 4. (a) A waveform from a strip-line recorded by the waveform readout board (DRS4). (b) Close-up of the rising part of the same waveform. The time pick-up in the leading-edge discriminator (d-LED) uses a fixed threshold, while the constant fraction discriminator (d-CFD) relies on the varied threshold with the pulse amplitude (A) and the fraction (f) coefficient.

and relative gains of the capacitor cells are calibrated. Since the detector output signal is negative polarity, the dynamic range is chosen to [-0.9, 0.1V] range by adjusting the offset voltage. Figure 5(a) shows the noise level of the readout board after the amplitude calibration. The RMS of the noise level is measured to 1.5 mV, which is higher than 0.35 mV in the DRS4 chip specification [17]. The on-board amplifier is thought to cause the noise level increase, and under investigation.

For timing calibration, Gaussian shape pulse having -250mV amplitude and 1.6 ns width is generated by using a Lecroy 9211 unit. The pulse is split by a T-connector, and fed to two input channels of the readout board. The different length of cables are used for two channels. From the fixed delay between channels, time differences between adjacent capacitor cells are determined. Since waveforms in the two channels are identical, m-LED method is used for the precise time difference measurement. The time calibration is carried out at the fixed sampling rate at 5 GS/s, at which the readout board runs to take coincidence data. After time calibration, the time difference between channels is measured, and the result is shown in Figure 5(b). From the distribution in the figure, 11 ps FWHM of time resolution is measured for the two channels. (Time resolution of single channel is estimated to 7.5 ps). This result is larger than ~7 ps FWHM using the DRS4 evaluation board (~3 ps) [14]. The higher noise level is expected to cause the worse time resolution.

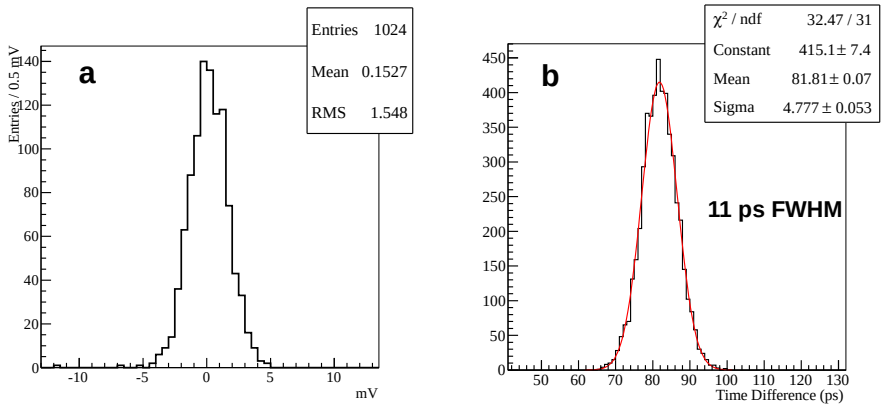

Figure 5. (a) noise level (~1.5 mV RMS) of 1024 capacitor cells in the waveform readout board. (b) Electronic time resolution ~11 ps FWHM is measured for two channels of the board.

3.2. Energy

The energy spectrum of 511 keV photon measured by a MCP PMT/TL module is shown in Figure 6(a). To obtain the energy of the strip, the area of the waveform is integrated for 150 ns from the pulse start. The energy of the module is the sum of the 15 strips, the photo-peak of the spectrum is normalized to 511 keV. The photo-peak is clearly separated from the Compton scattering, and the energy resolution at 511 keV is measured to be ~16.7% (FWHM). Figure 6(b) shows the energy profile measured in the 15 strips. The photo-peak events in [400, 650]keV are selected, and the energy fraction of the strip is normalized by the energy sum. The signal spread across the strips is ~ 8 mm in FWHM, which is larger than the crystal dimension.

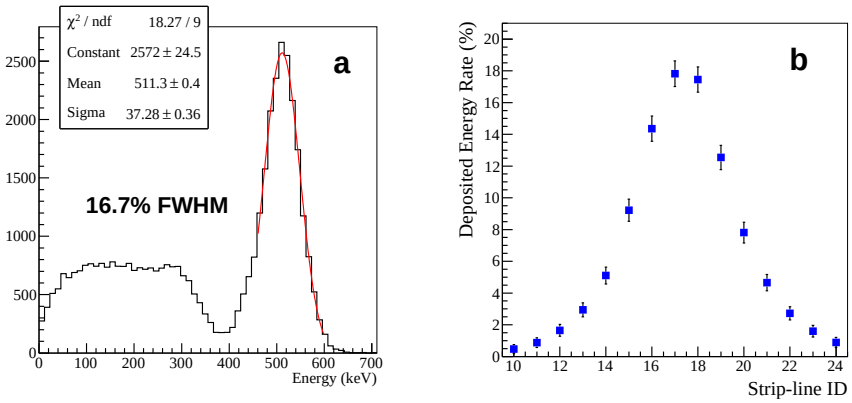

Figure 6. (a) Pulse-height spectrum of 511 keV annihilation photon measured by a MCP PMT/TL module. 15 strip-line signals are summed-up and the photo-peak is normalized to 511 keV. (b) Energy profile measured in 15 strip-lines from the 511 keV photo-peak events.

3.3. Coincidence Time

The coincidence time between the MCP PMT/TL module and R9800 PMT is measured for events in the photo-peak; the energy of the MCP PMT/TL module is obtained by summing-up energies from 15 strip-lines, and photo-peak events with [400, 650] keV energy for both modules are selected for the coincidence time measurement. To determine the event time for each strip-line, the d-LED and d-CFD threshold are applied on the rising part of the waveform. Figure 7(a) shows the differential time of two detector modules. The coincidence time resolution is measured to be ~370 ps (FWHM) from Gaussian fit. The result shown in the figure is obtained by applying the d-LED method with 8 mV threshold to the six highest energy strips (#15, 16, 17, 18, 19, 20 in Figure 6(b)); the average of six strips is taken as the event time for the MCP PMT/TL module. The time resolution dependence on the threshold is measured by varying the applied thresholds in d-LED, and is shown in Figure 7(b). The result shows that the best coincidence time resolution is achieved at lower threshold, and the time resolution becomes worse as the threshold increases. Similar tendency is observed in the result using the d-CFD time pick-up method.

3.4. Position

The crystal position perpendicular to the strip-line direction is obtained from the signal spread by

$$y = \sum_i e_i y_i / \sum_i e_i, \tag{1}$$

wheree_i and y_i is the partial energy and positions of the ith strip, respectively. The position measurement at two different crystal locations is shown in Figure 8(a). For this measurement, two LYSO crystals (3x3x10 mm^3) are placed next to each other, and energy window [400, 650] keV is required for photo-peak events. At each location, the position is determined precisely with ~0.46 mm FWHM resolution.

The crystal position along the strip-line is inferred from the differential time measured at both ends of the strip. The highest energy strip (#17 in Figure 6) is used for the measurement. Figure 8(b) shows the differential time measured

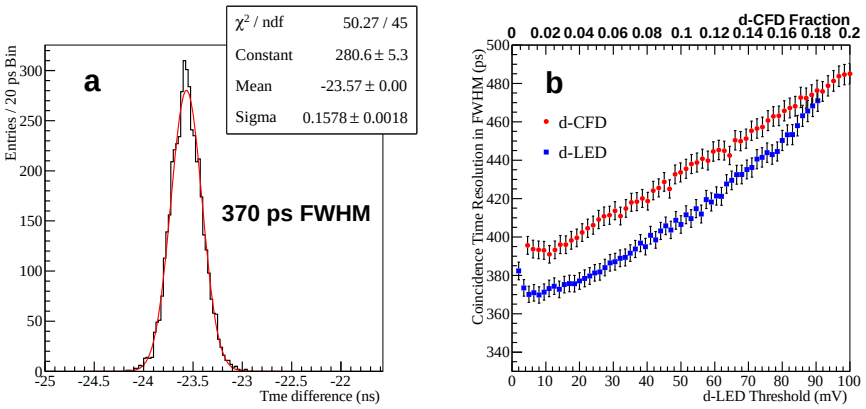

Figure 7. (a) Differential time between the MCP PMT/TL module and R9800 PMT in 511 keV photo-peak events. ~370 ps FWHM of coincidence time resolution is obtained by applying the d-LED with 8 mV threshold. (b) Coincidence time resolution dependence on the applied threshold in d-LED and on the fraction in d-CFD.

at two different locations along the strip-line. The two LYSO crystals are separated 20 mm from each other on the strip-line. The position resolution along the strip is inferred to be ~2.8 mm FWHM from ~40 ps of the differential time resolution and the signal propagation speed on the strip (0.46 c). The distance between two crystals calculated from the time difference is ~16.4 mm, which is smaller than the actual distance, 20 mm. An effect due to the LYSO crystal area (3x3 mm^2) might be one of the possible reasons of the difference. The investigation is underway by using a computer controlled positioning stage with 2.5 μm precision to localize the injection of 511 Kiev gamma into the LYSO crystal.

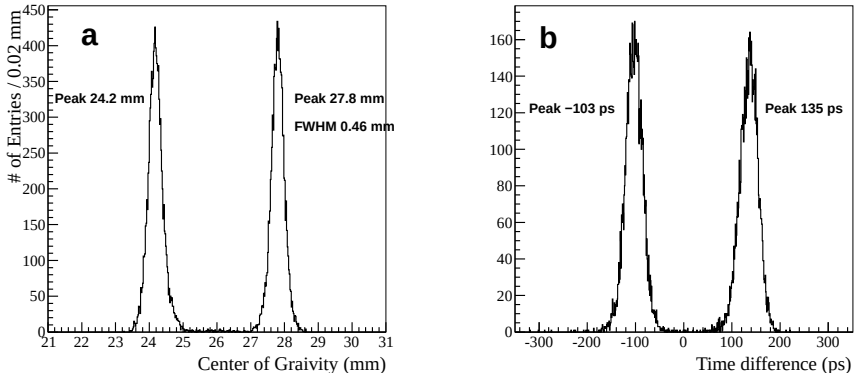

Figure 8. (a) Crystal position perpendicular to the strip-line direction is calculated from the strip-line coordinates weighted with their energies; ~0.46 mm FWHM for the position resolution is measured. (b) Differential time measured at two LYSO. ~2.8 mm FWHM is inferred from ~40 ps of the differential time resolution.

4. Summary

We have developed PET detector modules using 2"x2" Photonis XP85022 MCP PMTs as a demonstration of large area flat panel MCP PMT based TOF PET. In the prototype module, transmission-line readout scheme is adopted to efficiently collect signals from the large area MCP PMT with smaller readout channels. For data acquisition, high-speed waveform sampling by using the DRS4 prototype boards is employed to ensure the fast time response of

MCP PMT and also to precisely determine the event time. For the experimental tests, each MCP PMT/TL module is optically coupled to single LYSO crystal (3x3x10 mm^3), and detector responses to 511 keV annihilation photon are measured using the data taken in coincidence mode. Preliminary results obtained from the experiments can be summarized as follows: ~16.7% of energy resolution at 511 keV, ~370 ps (FWHM) coincidence time resolution, and position resolution of ~2.8 mm (0.46 mm) (FWHM) along (perpendicular to) the strip-line. This preliminary results demonstrate that the proposed detector technology is applicable to TOF PET, and works to make the modules more realistic (e.g., using array of scintillators) is underway.

Acknowledgments

This work was supported in part by the HEP Division of Argonne National Laboratory, a U.S. Department of Energy Office of Science laboratory, operated under Contract No. DE-AC02-06CH11357, the NIH grant R21 CA131639-02, and a seed grant provided by the Women's Board of the University of Chicago.

References

References

[1] W. Moses, Nucl. Instr. and Meth. **580** (2007) 919.
[2] M. Conti, Eur J Nucl Med Mol Imaging **38** (2011) 1147.
[3] S. Surti, A. Kuhn, M. Werner, A. Perkins, J. Kolthammer, J. Karp, J Nucl Med. **48** (2007) 471.
[4] B. Jakoby *et al.*, IEEE NSS/MIC Conference Record (2008) 3738.
[5] J. L. Wiza, Nucl. Instr. and Meth. **162** (1979) 587.
[6] K. Inami, N. Kishimoto, Y. Enari, M. Nagamine, T. Oshima, Nucl. Instr. and Meth. **560** (2006) 303.
[7] J. Va'vra, D. W. G. S. Leith, B. Ratcliff, E. Ramberg, M. Albrow, A. Ronzhin, C. Ertley, T. Natoli, E. May and K. Bryum, Nucl. Instr. and Meth. **A 606** (2009) 404.
[8] A. Lehmann *et al.*, Nucl. Instr. and Meth. **595** (2008) 173.
[9] The Large-Area Picosecond Photo-detectors Project web page. http://psec.uchicago.edu/
[10] J. Anderson, K. Byrum, G. Drake, C. Ertley, H. Frisch, J.-F. Genat, E. May, D. Salek and F. Tang, IEEE NSS/MIC Conference Record (2008) 2478-2481.
[11] J.-F. Genat, G. Varner, F. Tang, H. Frisch, Nucl. Instr. and Meth. **607** (2009) 387.
[12] H. Kim, H. Frisch, C.-M. Kao, C.-T. Chen, J.-F. Genat, F. Tang, W.W. Moses, W.S. Choong, Nucl. Instr. and Meth. **622** (2010) 628.
[13] http://www.photonis.com
[14] H. Kim, C.-T. Chen, H. Frisch, F. Tang, C.-M. Kao, Nucl. Instr. and Meth. **662** (2012) 26.
[15] S. Ritt, R. Dinapoli, U. Hartmann, Nucl. Instr. and Meth. **623** (2010) 486.
[16] C. W. Ueberhuber, Numerical Computation, Springer, Berlin, 1997
[17] DRS4 chip web page. http://drs.web.psi.ch/docs/DRS4_rev09.pdf